Int. J. Radiation Oncology Biol. Phys., Vol. 63, No. 5, pp. 1427–1431, 2005

0360-3016/05/$–see front matter

ELSEVIER

doi:10.1016/j.ijrobp.2005.05.034

CLINICAL INVESTIGATION **Lung**

CLINICAL OUTCOMES OF A PHASE I/II STUDY OF 48 Gy OF STEREOTACTIC BODY RADIOTHERAPY IN 4 FRACTIONS FOR PRIMARY LUNG CANCER USING A STEREOTACTIC BODY FRAME

YASUSHI NAGATA, M.D., PH.D., KENJI TAKAYAMA, M.D., YUKINORI MATSUO, M.D., YOSHIKI NORIHISA, M.D., TAKASHI MIZOWAKI, M.D., PH.D., TAKASHI SAKAMOTO, M.D., MASATO SAKAMOTO, M.D., MICHIHIDE MITSUMORI, M.D., PH.D., KEIKO SHIBUYA, M.D., NORIO ARAKI, M.D., SHINSUKE YANO, PH.D., AND MASAHIRO HIRAOKA, M.D., PH.D.

Department of Therapeutic Radiology and Oncology, Kyoto University, Graduate School of Medicine, Sakyo, Kyoto, Japan

Purpose: To evaluate the clinical outcomes of 48 Gy of three-dimensional stereotactic radiotherapy in four fractions for treating Stage I lung cancer using a stereotactic body frame.

Methods and Materials: Forty-five patients who were treated between September 1998 and February 2004 were included in this study. Thirty-two patients had Stage IA lung cancer, and the other 13 had Stage IB lung cancer where tumor size was less than 4 cm in diameter. Three-dimensional treatment planning using 6–10 noncoplanar beams was performed to maintain the target dose homogeneity and to decrease the irradiated lung volume >20 Gy. All patients were irradiated using a stereotactic body frame and received four single 12 Gy high doses of radiation at the isocenter over 5–13 (median = 12) days.

Results: Seven tumors (16%) completely disappeared after treatment (CR) and 38 tumors (84%) decreased in size by 30% or more (PR). Therefore, all tumors showed local response. During the follow-up of 6–71 (median = 30) months, no pulmonary complications greater than an National Cancer Institute-Common Toxicity Criteria of Grade 3 were noted. No other vascular, cardiac, esophageal, or neurologic toxicities were encountered. Forty-four (98%) of 45 tumors were locally controlled during the follow-up period. However, regional recurrences and distant metastases occurred in 3 and 5 of T1 patients and zero and 4 of T2 patients, respectively. For Stage IA lung cancer, the disease-free survival and overall survival rates after 1 and 3 years were 80% and 72%, and 92% and 83%, respectively, whereas for Stage IB lung cancer, the disease-free survival and overall survival rates were 92% and 71%, and 82% and 72%, respectively.

Conclusion: Forty-eight Gy of 3D stereotactic radiotherapy in 4 fractions using a stereotactic body frame is useful for the treatment of Stage I lung tumors. © 2005 Elsevier Inc.

Stereotactic body radiotherapy, Conformal radiotherapy, Lung cancer, Stereotactic body frame, Stereotactic radiotherapy.

INTRODUCTION

Stereotactic radiotherapy (SRT) for extracranial tumors has been recently performed to treat primary and secondary lung cancer and has subsequently been named stereotactic body radiotherapy. The advantages of hypofractionated radiotherapy for treating lung tumors are a shortened treatment course that requires fewer trips to the clinic than a conventional program and the adoption of a smaller irradiated volume allowed by greater setup precision. The disadvantages are uncertain effects of altered fractionation and the theoretical risk of worsening the ratio of normal tissue to tumor tissue through the use of a high dose per fraction. We previously published our setup accuracy (1), initial clinical results (2), computed tomography (CT) change after SRT (3), positron emission tomography (PET) evaluation after SRT (4) and treatment planning for SRT (5). In this study, the clinical results of lung cancer on our initial 5 years' worth of experiences are evaluated.

METHODS AND MATERIALS

Stereotactic radiotherapy was started for patients with lung tumor in July 1998 at Kyoto University. An integrated radiother-

Reprint requests to: Yasushi Nagata, M.D., Dept. of Therapeutic Radiology and Oncology, Kyoto University, Graduate School of Medicine, Sakyo, Kyoto, 606-8507, Japan. Tel: (+81) 75-751-3762; Fax: (+81) 75-751-3418; E-mail: nag@kuhp.kyoto-u.ac.jp

This work was partly presented at the 46th Annual Meeting of American Society for Therapeutic Radiology and Oncology (ASTRO), October 3–7, 2004, Atlanta, GA.

Supported by Grants-in-Aid No. 13470183, and 16390336 from the Ministry of Education and Science and No. 23765293 from the Ministry of Health, Welfare, and Labor in Japan.

Acknowledgments—The authors gratefully acknowledge Mr. Daniel Mrozek for his editorial assistance.

Received Feb 1, 2005, and in revised form May 20, 2005. Accepted for publication May 21, 2005.

apy system, including a CT simulator (CT-target, Shimadzu Corp., Kyoto, Japan), a three-dimensional (3D) radiotherapy treatment planning (RTP) machine (CADPLAN Ver 3.1, ECLIPSE Ver 7.1, Varian Associates, Palo Alto, CA), and a linear accelerator (CLINAC 2300C/D, Varian Associates) were in clinical use, and, in 1998, a stereotactic body frame (Stereotactic Body Frame, Elekta Corp., Stockholm, Sweden) was introduced for stereotactic body radiotherapy (SBRT).

Patients were fixed in the stereotactic frame (6, 7) using a vacuum pillow, and thereafter, six points were marked on the anterior chest wall with a laser marker and Indian ink. Then, respiratory movement of the tumor was observed with an X-ray simulator, where it was regulated when it was larger than 8 mm in the craniocaudal direction. A device called a diaphragm control, which is a board that pushes against the epigastric abdominal wall, was used for respiratory control. Serial CT scanning with 1 to 3 mm intervals around the tumor was performed over 4 s per slice without using the breath-hold technique. After the patient left the room, the target outlines of internal target volume (ITV) were drawn using the RTP machine. Our CT images included the respiratory movement of the target. Therefore, ITV including internal margins with clinical target volume (CTV) was delineated. ITVs and CTVs were not edited for anatomy. The setup margins between ITV and planning target volume (PTV) were 5 mm for the anteroposterior, 5 mm for the lateral, and 8–10 mm for the craniocaudal directions. Selection of the optimal direction of noncoplanar beams or dynamic arcs was performed by three experienced oncologists and technologists with the goal of the RTP being 6 to 10 portals for noncoplanar static beams. The beam energy used was 6 MV and the isocenter was single for all beams. All patients received four single treatments with 12 Gy of radiation prescribed at the isocenter. The mean ITV volume was 13 mL. The target dose homogeneity of ITV was within 20%, and the irradiated lung volume for >20 Gy (V20) was made as small as possible. As a result, the minimal and maximal ITV dose per fraction was 92% and 102.6%, respectively. The V20 ranged from 0.3% to 11.6% with a mean value of 4.3%. The irradiated dose–volume histograms of the other organs at risk, including the spinal cord, pulmonary artery, bronchus, and heart were also calculated. As a result, the mean and maximal single dose per fraction was 0.5 and 1.9 Gy for esophagus, 0.8 and 1.8 Gy for bronchus, 0.8 and 2.6 Gy for pulmonary artery, 0.3 and 2.7 Gy for heart, and 0.1 and 0.5 Gy for spinal cord, respectively (5). The target reference point dose was defined at the isocenter of the beam.

Before each treatment, anteroposterior and lateral portal films were taken for verification. The position of each patient was verified by three experienced oncologists and technologists at each treatment time. When the setup error was larger than 2 mm between the X-ray simulation film and portal film in any direction, the patient was repositioned and portal films were taken and verified again. Fractionated radiotherapy was performed with 4 days of 12 Gy over 5 to 13 (median = 12) days.

Using a linear-quadratic model (8), the biologic effective dose (BED) was here defined to be $nd\,(1+d/\alpha-\beta)$ Gy, where n is the fractionation number, d is the daily dose, and the α-β ratio was assumed to be 10 for tumors. The value was 105.6 Gy-BED for 48 Gy in four fractions (our study).

Forty-five patients with histologically confirmed Stage I primary lung cancer were treated between September 1998 and February 2004. Of them, 32 patients were Stage IA (T1N0M0); the other 13 were Stage IB (T2N0M0). Thirty-three patients were males and 12 were females, respectively. Their ages ranged between 51 and 87 years, and 77 years was the median for Stage IA, whereas they ranged between 68 and 80 years with 73 years as the median for Stage IB. Sixteen Stage IA patients were inoperable and the other 16 were operable but refused surgery, whereas 11 of the Stage IB patients were inoperable and the other 2 refused surgery. The histologies of the Stage IA patients were 16 squamous cell carcinoma, 15 adenocarcinoma, and 1 non–small-cell cancer and the Stage IB histologies were 8 squamous cell carcinoma and 5 adenocarcinoma.

The follow-up period was 6 to 71 (median = 30) months for the Stage IA patients and 6 to 61 (median = 22) months for Stage IB patients.

The eligibility criteria for the patients for Stage I primary lung cancer were *(1)* surgery was contraindicated or refused, *(2)* the patient could remain stable in the body frame for longer than 30 min (World Health Organization performance status ≤2), *(3)* oxygen was not required under normal conditions, *(4)* no active interstitial pneumonitis, and *(5)* written informed consent was obtained.

All patients were staged by bronchoscopy, CT, and after 1999 18-fluoro-deoxy-glucose (FDG)-PET scanning. The initial CT-based stage was changed in 2 patients with FDG-PET. For follow-up after the SRT, chest films were taken every month, and CT films were taken every 2 to 4 months for the first year and every 6 months between 1 year and 5 years after treatment. Toxicity was evaluated using the National Cancer Institute-Common Toxicity Criteria (NCI-CTC) Version 2.0.

Local tumor response was evaluated using the Response Evaluation Criteria in Solid Tumors criteria (9). Differentiation between radiation pneumonitis and residual tumor is difficult. However, new irregular densities which appeared within radiation field 2 to 6 months after radiotherapy and were thereafter reduced in size were considered to be radiation pneumonitis. All cases whose tumors decreased in size by 30% or more after radiotherapy were classified as PR. The cumulative survival rates were calculated using the Kaplan-Meier method.

RESULTS

Local tumor response

Of the 45 tumors, 7 (6 T1, 1 T2) (16%) completely disappeared after treatment (CR) and 38 (84%) decreased in size by 30% or more (PR). Also, all tumors showed a local response, but the distinction between tumor control from therapeutic effect was difficult. We considered any residual density surrounding a tumor after radiotherapy to be PR, and therefore the pathologic CR rate may have been much higher than 16%. During the follow-up, only one local failure that may be considered either marginal failure or regional nodal failure was encountered at 24 months, as shown in Fig. 1.

Toxicities

No severe symptomatic pulmonary complications (NCI-CTC Grade 3 or larger) were encountered. However, 2 patients (4%)—1 with T1 and the other with T2—received steroids after symptomatic pneumonitis and were categorized as NCI-CTC Grade 2. CT exams every 2 to 4 months after SRT showed mild pulmonary CT changes (NCI-CTC Grade 1) in the other 43 (96%) cases. Symptoms such as a

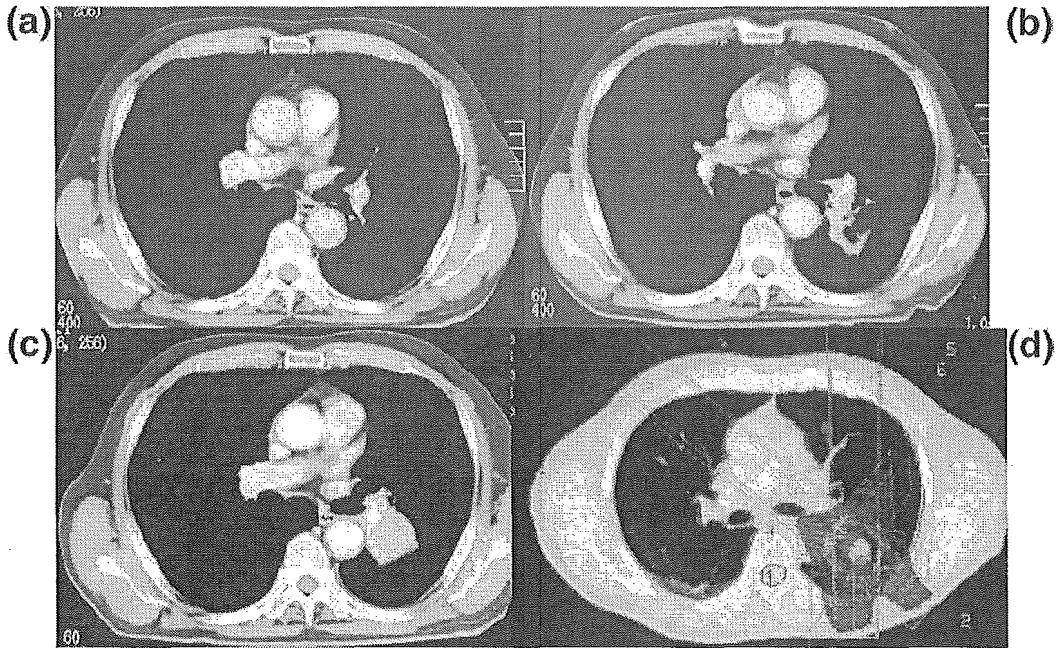

Fig. 1. A case of T1N0M0 lung cancer showing recurrence after stereotactic radiotherapy (SRT). The computed tomography images at 7 months (b, upper right) after SRT demonstrated a new soft-tissue density as well as radiation-induced lung damage (RILD) in the marginal area of the SRT that could not be observed at 2 months (a, upper left) after SRT. Initially, the density was considered to be RILD. However, the density increased in size at 16 months (c, lower left). The tumor was finally diagnosed as a local failure from either marginal failure or regional lymph nodal failure. The dose distributions are also shown (d, lower right).

mild cough, general malaise, and slight fever were present in 10 patients (22%) and were relieved without steroids at the outpatient clinic. A CT change in the liver was temporarily observed with the transient elevation of liver enzymes in a patient with a tumor in the right lower lung. As a result, no vascular complications, cardiac complications, esophageal complications, or neurologic complications were encountered.

Survival

T1N0M0 (Stage IA) primary lung cancer. For the 32 patients with histologically confirmed T1N0M0 Stage IA primary lung cancer, all but one of the tumors were locally controlled during the follow-up period. In 1 patient, a tumor locally recurred 24 months after SRT. In 3 patients, cancer recurred in regional hilar or mediastinal lymph nodes after 6, 12, and 24 months; in 4 patients, lung metastases after 2, 3, 20, and 55 months; and in the remaining patient, bone metastases were noted after 15 months without local recurrence. One patient died during the follow-up period from intercurrent causes.

Thus, the 1-year and 5-year local relapse-free survival rates were 100% and 95% as shown in Fig. 2. The disease-free survival rates after 1, 2, 3, and 5 years were 80%, 72%, 72%, and 72%, respectively, and the overall survival rates were 93%, 90%, 83%, and 83%, respectively.

T2N0M0 (Stage IB) primary lung cancer. Of the 13 patients with T2N0M0 Stage IB primary lung cancer, all tumors were locally controlled during the follow-up period. In 2 patients, cancer recurred distantly in the lung after 7 and 52 months, in 1 patient brain metastasis occurred after 10 months, and in the remaining patient liver metastases was noted after 12 months without local recurrence. Two patients died during the follow-up period from intercurrent causes.

Thus the 1- to 5-year local relapse free survival rates were also 100%. The disease-free survival after 1, 2, 3, and 5 years were 92%, 71%, 71%, and 71%, respectively, and the overall survival rates were 82%, 72%, 72%, and 72%, respectively, as shown in Fig. 3.

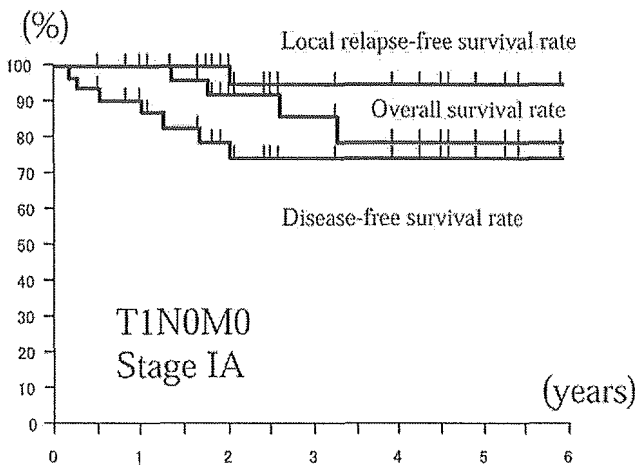

Fig. 2. The overall, local relapse-free, and overall disease-free survival rates of the patients with Stage IA (T1N0M0) lung cancer.

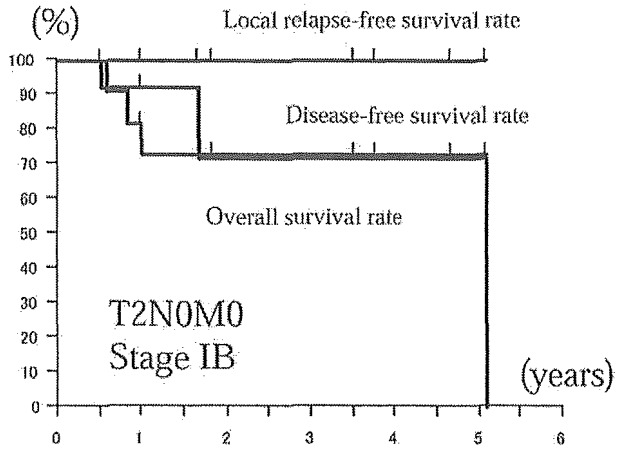

Fig. 3. The overall, local relapse-free, and overall disease-free survival rates of the patients with Stage IB (T2N0M0) lung cancer.

DISCUSSION

Local control rates of primary lung cancer with SRT has been previously reported by several authors: 94% (47/50) for 50 to 60 Gy in five fractions with a median follow-up of 36 months (10), 92% (22/24) for 60 Gy in eight fractions with a median follow-up of 24 months (11), 87% (30/37) for 60 Gy in three fractions with a median follow-up of 15 months (12), 85% for 48 to 60 Gy in eight fractions with a median follow-up of 17 months (13), 95% for 45 to 56.2 Gy in three fractions with a median follow-up of 10 months (14), and 97% (44/45) for 48 Gy in four fractions with a median follow-up of 22 to 30 months (as shown in Table 1 in this study). Using a linear-quadratic model with an α-β ratio = 10, our fractionation of 12 Gy × 4 was equal to 2 Gy × 44 = 88 Gy. A BED larger than 100 Gy may be effective for STI of solitary lung cancer with a local control rate of more than 85%. Timmerman (12) concluded that a 60 Gy marginal dose in three fractions is the limiting dose. Considering our clinical results, a further dose escalation study of more than 48 Gy in four fractions is not necessary for tumors smaller than 4 cm in diameter.

The current standard choice for Stage IA lung cancer treatment is lobectomy (15). However, for many patients this is not indicated because of accompanying diseases, such as chronic obstructive pulmonary disease, cardiac disease, and diabetes. For them, various minimal surgical techniques are indicated, including wedge resection and video-assisted thoracoscopic surgery as well as ablation. The local control rates of various other modalities for primary Stage I lung cancer previously reported was 93% for wedge resection and 83–95% for VATS and the 5-year survival rates were 82% and 50–70%, respectively (16).

Onishi (17) recently reported results for 13 institutions in Japan, where they summarized 245 patients, 155 with Stage IA lung cancer and 90 with Stage IB lung cancer. The operable and inoperable patients totalled 87 and 158, respectively, and their results showed that the intercurrent death rate was especially high in the inoperable patient group. Moreover, the 5-year survival rates of operable patients irradiated with more than BED = 100 Gy was 90% for Stage IA and 84% for Stage IB, and their clinical results were as good as those for surgery.

During our follow-up, no serious complications were encountered, and only mild radiation pneumonitis (NCI-CTC Grade 2 or less) was detected by CT. Graham (18) reported that the tolerance of the pulmonary dose >20 Gy (V20) is 25% of the whole lung with low risk. Our >20 Gy irradiated volume (V20) of the whole lung was 1.0% to 11.6% (average = 4.5%), which was markedly smaller than that in their report. However, the V20 of the standard fraction with 2 Gy and that of the SRT with 12 Gy must be different. Further close follow-up is required. Another concern of our study was the effects on the central bronchus, pulmonary artery, esophagus, heart, and spinal cord. The effects of the hypofractionated dose on the main bronchus, pulmonary artery, heart, and esophagus have not been followed for a long enough time. For our clinical experiences thus far, no severe complications have been encountered. However, lethal pulmonary bleeding and esophageal ulcer have been previously reported by other institutions (19). A case with a skin ulcer that finally caused thoracocutaneous fistula and another case with acute cholecystitis due to abdominal press were reported in Japan. Therefore, long-term follow up is still necessary.

Considering the tumor control dose, after dose escalation from 40 Gy to 48 Gy, only one local recurrence was encountered for primary lung cancer, and no severe complications were encountered for all tumors. Therefore, we will continue this schedule for the treatment of primary lung cancer. Systemic chemotherapy may be considered when the local tumor is well controlled and regional/distant metastases are frequent. On the other hand, the underlying pulmonary diseases could be a limiting factor for SRT of a solitary lung tumor. However, this should be discussed for each case. In our cases, 1 patient who had severe interstitial pneumonitis died of progression of pneumonitis 6 months after SRT. Because the occurrence of this pneumonitis was far distant from the irradiated tumor in the opposite lung, death was considered to be unrelated to the treatment. However, the effect of the scattered radiation dose cannot be completely neglected and the indications of SRT for the patients with interstitial pneumonitis should be limited. Our current indications are that a patient does not require oxygen under normal conditions and has no active interstitial pneumonitis shadow on a chest X-ray film. If these requirements are satisfied, this treatment can be performed without serious complications.

Recently, we started a multi-institutional Phase II study for T1N0M0 non–small-cell lung cancer under Japan Clinical Oncology Group (http://www.jcog.jp/) number 0403. Sixteen institutions have entered together and started the same dose SBRT with 48 Gy at the isocenter in four fractions for T1N0M0 lung cancer. The results of SRT for inoperable and operable Stage I lung cancer patients are awaited.

Table 1. Clinical results of stereotactic radiotherapy for primary lung cancer

Author (year)	Total dose (Gy)	Daily dose (Gy)	Reference point	Local control	Median follow-up
Uematsu (2001)	50–60	10	80% margin	94% (47/50)	36 months
Arimoto (1998)	60	7.5	Isocenter	92% (22/24)	24 months
Timmerman (2003)	60	20	80% margin	87% (30/37)	15 months
Onimaru (2003)	48–60	6–7.5	Isocenter	80% (20/25)	17 months
Wulf (2004)	45–56.2	15–15.4	80% margin	95% (19/20)	10 months
This study (2005)	48	12	Isocenter	97% (44/45)	30 months

The primary indication for stereotactic radiotherapy in lung cancer could be a Stage Ia (T1N0M0) patient. Very early stage lung cancer can now be detected by screening CT examination, and these cases are also good indications for SRT. However, the issue of these cases is histologic confirmation. In our clinical experience, 7 of 95 total SRT cases could not be finally confirmed histologically. Of course, these seven cases are not included in this study. They could not be histologically confirmed because of the failure or difficulty in CT-guided biopsy or transbronchoscopic lung biopsy. CT screening has revealed very early staged lung cancer with ground glass opacity and some patients with severe emphysema could be contraindicated for biopsy. Therefore, the indication for SRT for these cases without histologic confirmation should be discussed in the future. When the tumor becomes larger than 3 cm in diameter, which corresponds to Stage Ib (T2N0M0), SRT is possible. However, the intratumor dose becomes less homogeneous, and the rate of occult distant metastases may increase. Therefore, the extension of the indication of this technique for T2 tumors requires more consideration for dose escalation or adjuvant chemotherapy.

CONCLUSION

The feasibility and accuracy of 3D conformal radiotherapy using a stereotactic body frame was evaluated. 3D SRT using a stereotactic body frame is a safe and effective treatment method for solitary lung tumors. Thus further clinical studies are warranted in future.

REFERENCES

1. Negoro Y, Nagata Y, Aoki T, *et al.* The effectiveness of an immobilization device in conformal radiotherapy for lung tumor: Reduction of respiratory tumor movement and evaluation of daily set-up accuracy. *Int J Radiat Oncol Biol Phys* 2001;50:889–898.
2. Nagata Y, Negoro Y, Aoki T, *et al.* Clinical outcomes of 3-D conformal hypofractionated single high dose radiotherapy for one or two lung tumors using a stereotactic body frame. *Int J Radiat Oncol Biol Phys* 52;1041–1046, 2002.
3. Aoki T, Nagata Y, Negoro Y, *et al.* Evaluation of CT appearance of lung injury after three-dimensional conformal stereotactic radiotherapy for solitary lung tumors. *Radiology* 2004; 230:101–108.
4. Ishimori T, Saga T, Nagata Y, *et al.* 18F-FDG and 11C-Methionine evaluation of the treatment response of lung cancer after stereotactic radiotherapy. *Ann Nuclear Med* 2004;18: 669–674.
5. Takayama K, Nagata Y, Negoro Y, *et al.* Treatment planning of stereotactic radiotherapy for solitary lung tumor. *Int J Radiat Oncol Biol Phys* 2005;61:1565–1571.
6. Blomgren H, Lax I, Goeranson H, *et al.* Radiosurgery for tumors in the body: Clinical experience using a new method. *J Radiosurg* 1998;1:63–74.
7. Lax I, Blomgren H, Larson D, *et al.* Extracranial stereotactic radiosurgery of localized target. *J Radiosurg* 1998;1:135–148.
8. Yaes RJ, Patel P, Maruyama Y. On using the linear-quadratic model in daily clinical practice. *Int J Radiat Oncol Biol Phys* 1991;20:1353–1362.
9. Therasse P, Arbuck SG, Eisenhauer EA, *et al.* New guidelines to evaluate the response to treatment in solid tumors. *J Natl Cancer Inst* 2000;92:205–216.
10. Uematsu M, Shioda A, Tahara K, *et al.* Computed tomography-guided frameless stereotactic radiotherapy for stage I non-small-cell lung cancer: A 5-year experience. *Int J Radiat Oncol Biol Phys* 2001;51:666–670.
11. Arimoto T, Usubuchi H, Matsuzawa T, *et al.* Small volume multiple non-coplanar arc radiotherapy for tumors of the lung, head, and neck and the abdominopelvic region. In: Lemke HU, editor. CAR '98 Computer assisted radiology and surgery. Tokyo: Elsevier; 1998. p. 257–261.
12. Timmerman R, Papiez L, McGarry R, *et al.* Extracranial stereotactic radioablation: Results of a phase I study in medically inoperable stage I non-small cell lung cancer. *Chest* 2003;124:1946–1955.
13. Onimaru R, Shirato H, Shimizu S, *et al.* Tolerance of organs at risk in small-volume, hypofractionated, image-guided radiotherapy for primary and metastatic lung cancers. *Int J Radiat Oncol Biol Phys* 2003;56:126–135.
14. Wulf J, Haedinger U, Oppitz U, *et al.* Stereotactic radiotherapy for primary lung cancer and pulmonary metastases: A noninvasive treatment approach in medically inoperable patients. *Int J Radiat Oncol Biol Phys* 2004;60:186–196.
15. Lung Cancer Study Group. Randomized trial of lobectomy versus limited resection for T1N0 non-small cell lung cancer. *Ann Thorac Surg* 1995;60:615–623.
16. Luketich JD, Ginsberg RJ. Limited resection versus lobectomy for stage I non-small cell lung cancer. In: Pass HI, Mitchell JB, Johnson DH, *et al.*, editors. Lung cancer: Principles and practice. Philadelphia: Lippincott-Raven; 1996. p. 561–566.
17. Onishi H, Araki T, Shirato H, *et al.* Stereotactic hypofractionated high-dose irradiation for stage I non-small cell lung carcinoma. *Cancer* 2004;101:1623–1631.
18. Graham MV. Predicting radiation response. *Int J Radiat Oncol Biol Phys* 1997;39:561–562.
19. Herfarth KK, Debus J, Lohr F, *et al.* Stereotactic single dose radiation treatment of tumors in the lung. *Radiology* 2000;217: 148.

ORIGINAL ARTICLE

Radiation Medicine: Vol. 23 No. 1, 14–24 p.p., 2005

Evaluation of Inter- and Intrafraction Organ Motion during Intensity Modulated Radiation Therapy (IMRT) for Localized Prostate Cancer Measured by a Newly Developed On-board Image-guided System

Keith R. Britton, Yoshihiro Takai, Masatoshi Mitsuya, Kenji Nemoto, Yoshihiro Ogawa and Shogo Yamada

Purpose: To investigate prostatic organ motion at both setup and intrafraction using an on-board image-guided system. An intrafraction field-based repositioning method also was evaluated.

Materials and Methods: A dual fluoroscopy with amorphous-silicon flat panel (DFFP) system was used for the three-dimensional registration of implanted markers in the prostate of eight organ-confined cancer patients planned for treatment with intensity modulated radiation therapy (IMRT). Day-to-day motion errors were quantified and intrafraction displacements of more than ±1 mm were corrected.

Results: Among 214 fractions and 565 system views, day-to-day mean magnitude of marker discrepancy±standard deviation (SD) was 1.76±1.4 mm, 3.14±1.6 mm, and 3.78±2.4 mm in the right-left, cranial-caudal, and anterior-posterior directions, respectively. The intra-fractional mean magnitude±SD of marker displacement was 0.45±0.7 mm, 1.08±1.38 mm and 1.45±1.70 mm in the right-left, cranial-caudal, and anterior-posterior directions, respectively. Intrafraction corrected sessions (84/214) showed a median (range) of motion of 0.1 mm (−1.2 to 0.7 mm), −0.2 mm (−2.1 to 1.1 mm), and −0.2 mm (−1.7 to 2.0 mm) in the right-left, cranial-caudal, and anterior-posterior directions, respectively.

Conclusion: Motion uncertainty can be considerably decreased with daily use of the DFFP system. Reduced intrafraction organ motion clearly endorsed the value of the repositioning approach, allowing a safer dose escalation protocol.

Key words: interfraction motion, intrafraction motion, image-guided radiation therapy, localized prostate cancer, intensity modulated radiation therapy (IMRT)

Introduction

The goal of all radiation therapy is to irradiate tumors with a lethal dose while limiting the radiation received by the normal tissue that surrounds the tumor. To date, increasing numbers of tumors have been treated with higher radiation doses while limiting high doses to critical structures. The development of three-dimensional conformal radiation therapy (3D-CRT) and intensity modulated radiation therapy (IMRT) has provided tools to account for geometrical uncertainties that affect optimization of the conformal plans. The treatment of prostate cancer patients however, presents a challenge to increasing the dose to best achieve tumor eradication.[1,2]

New technology has arisen for decreasing treatment errors arising from tumor delineation, organ motion, and daily patient positioning so that therapy can be delivered safely, accurately, and with fewer time-consuming steps. This includes sequential CT acquisitions,[3,4] portal image acquisitions,[5-8] MRI,[9] ultrasound (US)[10-14] and fluoroscopy-based fiducial marker-guided radiation therapy.[15,16]

Accounting for treatment errors including random error (variation of a landmark's position about its mean value), systematic error (average displacement of a landmark's position relative to its position at simulation), and volume changes (time trends) is an increasingly

Received April 14, 2004; revision accepted June 20, 2004.

Department of Radiation Oncology, Tohoku University Graduate School of Medicine

Reprint requests to Yoshihiro Takai, M.D., Department of Radiation Oncology, Tohoku University Graduate School of Medicine, 1-1 Seiryo-machi, Aoba-ku, Sendai, Miyagi 980-8574, JAPAN.

important part of the clinical radiation therapy process. Therefore, knowledge of treatment errors, their characteristics, and possible techniques for reducing them need to be prioritized when modeling the radiation therapy process. In the case of prostate IMRT, there has been a great deal of effort to better shape high dose distributions, with physicists and engineers making most of this effort. Interfraction and intrafraction organ motion measurements have direct implications for the size and design of planning target volume (PTV).

Techniques for decreasing treatment geometrical errors have been implemented widely for many years,[5,17,18] with experiences varying according to strategies used. These procedures include variables such as patient immobilization style, treatment position, rectum or bladder filling, and the use of "gold standard" images or newer imaging systems at the time of simulation or during treatment fractions.

At our institution, an advanced clinical and technological method has been put into use to overcome some of the past limitations of irradiation of organ-confined prostate cancer and, hence, to increase the probability of higher local tumor control.

Although it is impossible to abolish all treatment uncertainty, knowledge of the actual extent of target motion is of paramount importance for implementing high dose escalation protocols and decreasing the extension of larger margins around the clinical target volume (CTV).

Fractionated radiation therapy treatments require patient positioning of about 35 times at similar planned positions. To achieve this goal, several techniques and imaging tools have been used, with most of them aiming to account for the uncertainty by increasing treatment margins[19] or by monitoring and controlling organ shift.[18,20]

This study focused on the measurement of interfraction (setup) and intrafraction (during delivery) organ motion. Organ motion was analyzed on the basis of real-time registration of the tri-dimensional (3D) position of internal markers implanted in the prostate. For this, a newly developed image-guided system was implemented to register, online, fiducial marker location distributions at megavoltage (MV) and kilovoltage (KV) X-ray energies using paired amorphous silicon (a-Si) flat panels mounted on a medical linear accelerator, namely, a dual fluoroscopy and flat panel (DFFP) system. In addition, the study was extended to the description of an intra-treatment field-based correction method.

Materials and Methods

At the Department of Radiation Oncology of Tohoku University Hospital, high dose irradiation using IMRT has been offered since January 2001. This technique has been implemented for the treatment of clinical and pathologically diagnosed adenocarcinoma of the prostate as a definitive treatment.

Table 1. Patient characteristics

Characteristic	Patients	(%)
Pre TX PSA		
<10	6	75
10-20	1	12.5
>20	1	12.5
Biopsy Gleason score		
2-6	0	0
7	7	87.5
8-10	1	12.5
Clinical stage		
$T1_c$	3	37.5
$T2_a$	2	25
$T2_b$	0	0
$T3_a$	2	25
$T3_c$	1	12.5
*Neo-adj. hormone therapy	8	100
Prescribed dose		
72 Gy	5	62.5
76 Gy	3	37.5
Age		
Median	72.6	
Range	63-78	

PSA = Prostate-specific antigen. * Applied 3-6 months before radiation treatment.

Defining patients and preparation characteristics

Patient selection

The data of a group of eight organ-confined prostate cancer patients selected for IMRT as the entire treatment was used for organ motion analysis. The patients' characteristics are shown in Table 1. For all patients, neoadjuvant hormone therapy was prescribed for three to six months before the start of treatment, as done and reported by other authors.[21-23] As patient selection criteria, we included those with a confirmed histological diagnosis of adenocarcinoma, classified according to the Gleason grading system,[24] with clinical stages from T1c to T3 according to the International Union Against Cancer (UICC).[25] In addition, negative lymph node status (N0) or negative metastatic status (M0) was required. All patients presented intermediate to high prognostic risk factors. An absolute rule was acceptable performance status (Karnofsky scale). The consent of all patients was obtained before the study was carried out.

Fiducial markers

Patients underwent transrectal ultrasound-guided implantation of three gold markers (Hakko guiding marker system), under local anesthesia, each one sized 3×0.8 mm for maximal position, reproducibility, and accuracy throughout the treatment period. After the insertion procedure, a week is given to check for any post-procedure inflammation or foreign body reaction sign. In addition, prophylactic antibiotic coverage is routinely prescribed to all patients. Markers were intended to be inserted at the base of the gland and/or at mid-gland position.

Radiation therapy and planning methods

Patient indications

Our patients underwent radiation therapy with restrictions on some specific dietetic components (those producing much intestinal gas). They were asked to avoid such foods on the day of CT image acquisition and subsequent treatment days. Because of the difficulty of eliminating all forms of motion uncertainty, we instructed the patients carefully in using constant ventilation cycles. In addition, all patients were asked to defecate every morning and to void the bladder 30 to 60 minutes before CT imaging and fraction delivery, so that partial bladder filling is obtained and large variations can be avoided, as recommended and reported by other authors.[17,26]

Immobilization

To achieve accurate patient positioning and reproducibility, patients were immobilized in the supine position with an individually fashioned whole-body vacuum cast that molds to the patient's external contours; this is fitted within an external whole-body frame (Fig. 1). Moreover, two over-hip belts were placed to prevent potential body-induced motion, even while recognizing the subjectivity of the method.

CT acquisition

Images for IMRT planning were obtained from the contrast-enhanced axial CT scan data of the patients. To improve soft tissue visualization and periprostatic vasculature, 1.25- to 2.5-mm slice intervals were used in target volumes and organs at risk (OAR) areas; the rest of the scan was taken with a slice interval of 5 mm up to 8-10 cm above and under the prostate gland. The images were transferred to an IMRT planning workstation (CADPLAN, VMS, Palo Alto, CA), where contours for the prostate, seminal vesicles, rectum, bladder, and femoral heads were outlined on each axial image by one physician (K.B.).

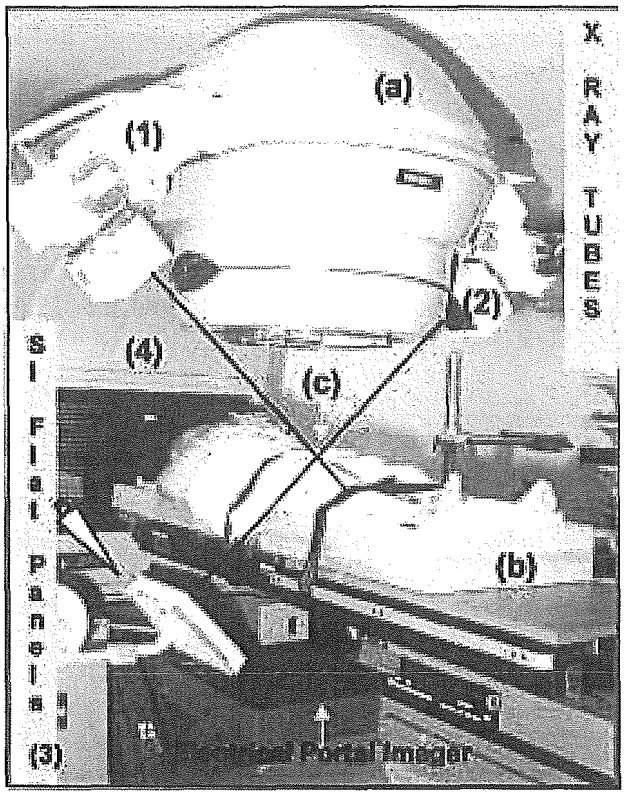

Fig. 1. Dual fluoroscopy and paired flat panel system (a). Typical (supine) patient setup positioning used for CT and image-guided IMRT with external body fixation frame and vacuum cast (b). Isocentered gold marker (GS-1-iso) is aligned at the intersection between kv ray beam axis and accelerator isocenter (c). Shown are X-ray tubes (1, 2), a-Si flat panels (3), and Linac (4). CT = computerized tomography, SI = silicon.

Planning methods

Inverse planning optimization software was used to create the intensity-modulated pattern with the CADPLAN (VMS, Palo Alto, CA) planning system. Target volume consisted of the prostate and entire seminal vesicles, referred to as the CTV. A margin of 5 mm in all directions was used to account for the PTV based on a preliminary approach where intrafractional motion was seen to be <5 mm in 100% of the right-left (R-L) axis and in 98% of the cranial-caudal (C-C) and anterior-posterior (A-P) axes.

The bladder was contoured as a whole structure; rectum outer wall, bilateral femoral heads, and gold markers were also outlined. Of the inserted gold seeds (GS), the nearest to the mid-gland or an intra-tumor seed was used as the target isocenter (GS-1-iso) and for positional verification purposes; markers were designated as GS-1-iso, GS-2, and GS-3. The beam arrangement consisted of five coplanar non-colinear fields in the transverse plane isocentered to GS-1-iso.

This arrangement consisted of a direct posterior field, with two oblique anterior (45 degrees apart from gantry 0 degrees) and two oblique posterior fields (75 degrees apart from gantry 180 degrees). Treatment delivery was made using a dynamic multileaf collimator (DMLC) and the sliding window technique. Radiation doses delivered for this study group (Table 1) were in the range of 72-76 Gy (depending on the pre-established phase I/II dose escalation protocol assigned) in 2 Gy per fraction to the ICRU 50 (International Commission on Radiation Units and Measurements)[27] point.

DFFP system

A new system installed in the gantry of a medical linear accelerator (Clinac 23 EX, VARIAN Medical Systems, Palo Alto, CA.) consisted of dual X-ray generators (RAD II simulator, Haynes Radiation, Ltd.) powered by high-frequency (32 kW) and paired a-Si flat panel imagers (PaxScan 2520, VARIAN, V.M.S., Palo Alto, CA) (Fig. 1). The active area of the detector comprises 1408×1888 pixels, resulting in an imaging area of 17.9×23.8 cm. The system was used for intrinsically recognizing the coordinates, in 3D, of the center of the implanted GS as the pixel positions in the a-Si flat panels by x-ray sensors, through computer-controlled steps. The flat panels operate at a frame time of 33 ms, with further imaging processing through digital video signals and video graphic array (VGA) monitors. Views are always taken from 0° (degrees) of the gantry. The values are quantified as the geographical coordinates of the markers and expressed as digital figures. The accuracy and stability of the system has been discussed in previous reports.[28-30]

Registration method

The localization and measurement of the implanted gold markers' 3D coordinates, day-to-day and from the beginning to the end of the fraction, confirmed the primordial base of the organ motion analysis, assuming stable, accurate reproducibility of the DFFP system images.

At the time of the start of each treatment fraction, the patient is aligned by the skin marks drawn with the laser localizer signal in the treatment room. An initial real-time fluoroscopic view of the GS-1-iso marker coordinates is taken in 3D and sent as digital figures to the DFFP system workstation. This measured target isocenter location is changed, if needed, to the prescribed position 0, 0, 0 (defined by the intersection between the system beam axis and the accelerator isocenter point). After this, electronic portal images (EPID, Portal vision aS 500, VMS, Palo Alto, CA) are taken in order to verify the first field's R-L, superior-inferior (C-C), and A-P axis margins as well as the GS-1-iso with an energy of 6 MV X-photons.

After the setup process, the gold marker coordinates are recorded either prior to every field delivery or every other field delivery for the on-line isocenter location and to maintain a predetermined shift range equal to or less than ±1 mm in any of the R-L, C-C, or A-P axes. Over the course of a fraction delivery, "off-range" (O-R) displacements were corrected by shifting the treatment couch to the initial coordinates as many times as necessary.

In this study, our interest was to measure the changes in target isocenter location and the daily accurate alignment between the radiation beam and the target isocenter at patient setup and throughout the treatment process.

The analysis of organ motion was carried out 1) by measuring each patient's corresponding isocenter shifts relative to the system isocenter position derived after the manual skin laser-guided setup. Shifts in the left, inferior, and posterior directions were counted as negative (−) direction axis and shifts to the right, superior, or anterior, as positive (+). Interfractional motion error was determined by the difference between the measured position (day-to-day isocenter position) and the system isocenter. For each patient, estimation of the average magnitude of displacement of the daily setup is the patient's systematic error (organ motion + setup error). These average values are represented along with their variations (1 SD). Reported data are given for each patient and also for the entire study group. The mean magnitude of displacement [average of the displacement error of each patient's treatment regardless of the direction sign (±) of shift], overall absolute magnitude (mean of all patients as a whole), SDs, overall SDs, and extreme (±) values of isocenter shifts were calculated for the whole study group. 2) In addition, successive calculations of target isocenter misalignments through the whole intrafraction period (total of 3-5 system views depending on case) were carried out for analysis of intrafractional (random) organ motion. This would enable repositioning when O-R isocenter shifts existed. Registered coordinates, until correction was seen as necessary, accounted for this analysis. Like the analysis done for day-to-day variations, the values for variations during treatment were expressed for each patient and for the entire group as the mean magnitude with variation (1 SD).

Furthermore, after the last fraction field was delivered, another registration of the isocentered gold marker was obtained by the system in order to assess the end-of-treatment location. Post-treatment organ motion is referred to as the markers position just after the end of treatment. At this point, motion ranges in the R-L, C-C,

Table 2. Prostate interfraction (organ + setup) discrepancy of target isocenter between daily measured position and DFFP system isocenter

	Right-left			Cranial-caudal			Anterior-posterior		
	Range	Mean magnitude (mm)	SD (mm)	Range	Mean magnitude (mm)	SD (mm)	Range	Mean magnitude (mm)	SD (mm)
1	{−0.3 to 5.7}	3.20	2.41	{−2.6 to 6.7}	4.00	2.19	{−2.1 to 2.8}	1.60	1.05
2	{−2.3 to 2.7}	1.40	0.70	{−2.5 to 3.2}	1.60	0.90	{−13.4 to −0.9}	9.00	3.50
3	{−10.5 to 6.0}	2.68	2.29	{−7.1 to −0.3}	3.87	1.99	{−5.3 to 4.6}	1.42	1.50
4	{−1.6 to 1.8}	0.83	0.61	{−8.6 to 0.0}	4.62	2.48	{−11.3 to 4.0}	3.36	3.20
5	{−1.9 to 5.7}	1.39	1.36	{−4.2 to 3.7}	1.77	1.25	{−4.2 to 12.1}	3.34	2.77
6	{−0.7 to 4.1}	1.77	1.16	{−6.3 to 0.3}	3.41	1.64	{−13.1 to 0.0}	6.59	2.97
7	{−2.3 to 4.6}	1.53	1.09	{0.0 to 9.3}	4.60	1.68	{−11.9 to 5.9}	3.48	3.02
8	{−1.0 to 9.0}	1.25	1.64	{−1.5 to 2.7}	1.23	0.78	{−3.5 to 5.7}	1.42	1.22
all	{−2.5 to 4.95}	1.76	1.41	{−4.6 to 3.2}	3.14	1.61	{−8.9 to 4.2}	3.78	2.40

Abbreviations: mm (millimeters); SD: standard deviation; range values represent extreme values of marker shift in each direction (±).

and A-P directions were evaluated by extreme (±) values and mean shifts.

The study of seed migration was not part of this analysis, nor were other sources of motion uncertainty, like possible leg or organ rotations or motion induced by pelvic components.

RESULTS

Interfraction organ motion

A total of 214 treatment fractions were analyzed. For patient's setup positioning and marker localization over the course of treatment, 565 DFFP system images of the implanted gold markers were acquired successfully, allowing for prospective positional verifications with a high degree of reliability. The DFFP system yielded high-resolution imaging of markers as well as referent anatomical structures.

Ranges, mean absolutes of shifts, and SDs of the isocenter positional distributions for all patients are displayed in Table 2. The mean magnitude of uncertainty in the R-L, C-C, and A-P directions were in the range of 0.83 mm to 3.20 mm, 1.23 mm to 4.62 mm, and 1.42 mm to 9.0 mm, respectively. The overall mean magnitude of isocenter displacement was 1.76 mm, 3.14 mm, and 3.78 mm in the R-L, C-C, and A-P directions, respectively. The overall SD of isocenter shifts were 1.4 mm, 1.6 mm, and 2.4 mm in the R-L, C-C, and A-P directions, respectively. As shown in Fig. 2, the absolute values of marker motion frequency were seen to be <5 mm in 96.3%, 78.6%, and 69.6% in the R-L, C-C, and A-P directions, respectively. On the other hand, misalignments higher than or equal to 8 mm were found in only 0.5%, 1%, and 12% in the R-L, C-C, and A-P directions, respectively.

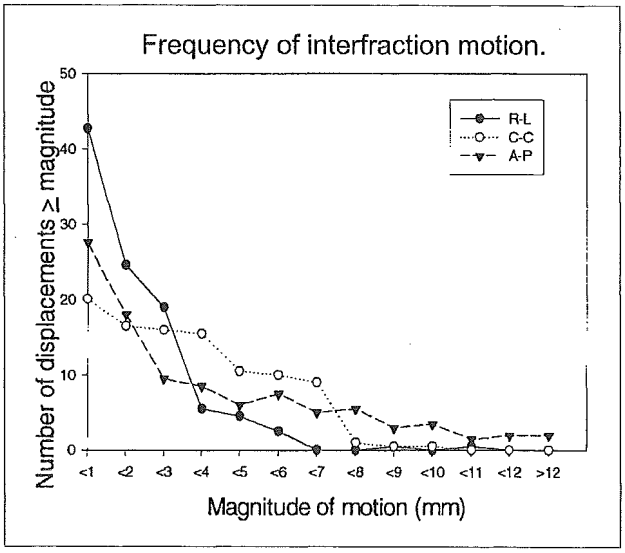

Fig. 2. Overall patients' interfractional target isocenter (GS-1-iso) frequency distributions relative to laser-skin marks, by axis. Right-left (R-L), cranial-caudal (C-C), and anterior-posterior (A-P).

Intrafraction organ motion/corrected fractions

The intrafraction marker positional distribution for all studied fractions is presented in Table 3. Marker positional corrections ("repositioning"), as described in registration methods, were necessary in 39.2% of the fractions studied (84/214). On the other hand, in the other 60.8% of fractions (130/214), repositioning was not required during the delivery process.

In this study, the overall median of organ intrafraction motion was 0.0 mm, 0.35 mm, and 0.65 mm in the R-L,

Table 3. Patients' intrafraction isocenter motion discrepancy for repositioned sessions

Patient	Left-right			Caudal-cranial			Posterior-anterior		
	Range	Mean magnitude (mm)	SD	Range	Mean magnitude (mm)	SD	Range	Mean magnitude (mm)	SD
1	{−1.4 to 4.4}	0.54	1.2	{−3.0 to 1.3}	0.83	1.1	{−3.0 to 5.0}	2.00	2.1
2	{−0.2 to 2.4}	0.68	0.9	{−7.5 to 1.4}	2.22	3.1	{−4.9 to 3.9}	2.50	3.2
3	{−1.9 to 0.2}	0.51	0.7	{−2.3 to 0.4}	1.17	1.1	{−1.3 to 2.1}	0.81	1.0
4	{−1.2 to 0.8}	0.58	0.7	{−0.6 to 2.1}	1.00	0.8	{−3.2 to 1.9}	1.31	1.7
5	{−1.4 to 1.2}	0.51	0.7	{−2.1 to 1.6}	1.17	1.2	{−1.5 to 2.5}	1.12	1.3
6	{−0.4 to 0.0}	0.20	0.2	{1.0 to 1.1}	1.05	0.0	{0.5 to 0.7}	0.60	0.1
7	{−0.5 to 0.7}	0.38	0.4	{−2.7 to 0.3}	1.43	0.9	{−2.0 to 1.1}	1.28	0.8
8	{−0.4 to 0.7}	0.26	0.2	{−2.2 to 0.9}	0.66	0.7	{−2.0 to −0.9}	1.33	0.3
all	{−1.9 to 4.4}	0.45	0.7	{−7.5 to 2.1}	1.08	1.38	{−4.9 to 5.0}	1.45	1.7

Abbreviations: (mm) = millimeter; SD = standard deviation; negative range values indicating shifts to the left (X), inferior (Y), or posterior (Z) directions. Range values are given in millimeters.

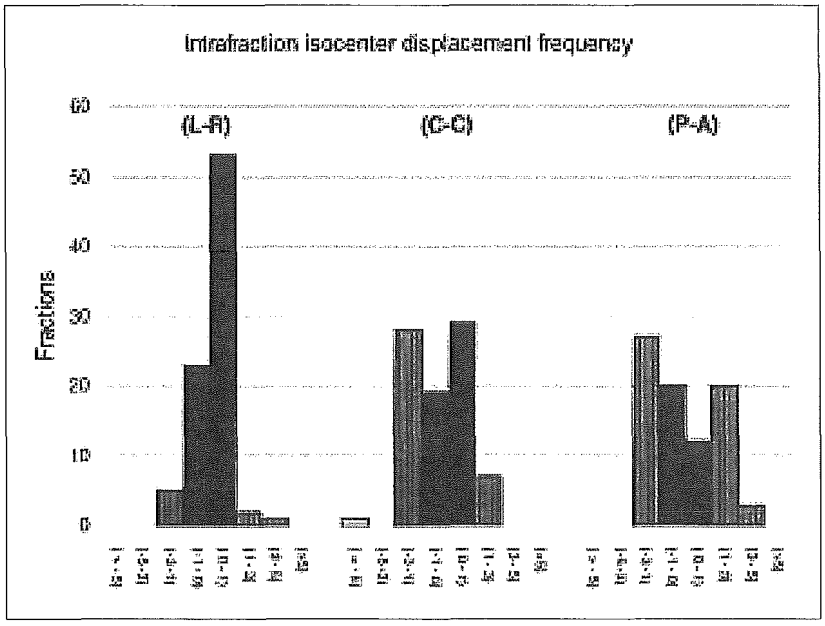

Fig. 3. Distribution of marker's coordinate shifts relative to prescribed isocenter position. Values in brackets are given in millimeters (mm); positive values and values with negative sign (–) refer to a shift towards the right, superior, and anterior for positive values, and left, inferior, and posterior for negative directions; "off-range" discrepancies in more than one axis, as registered by the DFFP system, are also plotted.

C-C, and A-P directions, respectively. Extreme maximums (±directions) and mean absolute values of discrepancy are presented in Table 3.

The overall mean magnitude of intrafraction marker shifts±SD was 0.45±0.7 mm, 1.08±1.38 mm, and 1.45±1.7 mm in the R-L, C-C, and A-P directions, respectively. The SD of target discrepancy ranged from 0.2 to 1.2 mm in the R-L direction, 0 to 3.1 mm in the C-C direction, and 0.1 to 3.2 mm in the A-P direction. The O-R marker shift frequency was found to be higher towards the C-C and A-P directions, as seen in >90% of repositioned fractions (Fig. 3). The frequency of O-R marker shifts by axis was 9.52%, 42.85%, and 61.90% in the R-L, C-C, and A-P directions, respectively. These results were derived from the registration of simultaneous O-R shifts in more than one axis at the same time (23%) for the repositioned fractions. The lateral axis was found to be fairly stable during most of the treatment sessions.

The actual marker discrepancy values [median (range)] under which treatment was delivered were 0.1 mm (–1.2-0.7 mm), –0.2 mm (–2.1-1.1 mm), and –0.2 mm (–1.7-2.0 mm) for the R-L, C-C, and A-P directions, respectively. As calculated regardless of the sign, the mean absolute values were 0.3 mm, 0.4 mm, and 0.44 mm for the R-L, C-C, and A-P directions, respectively.

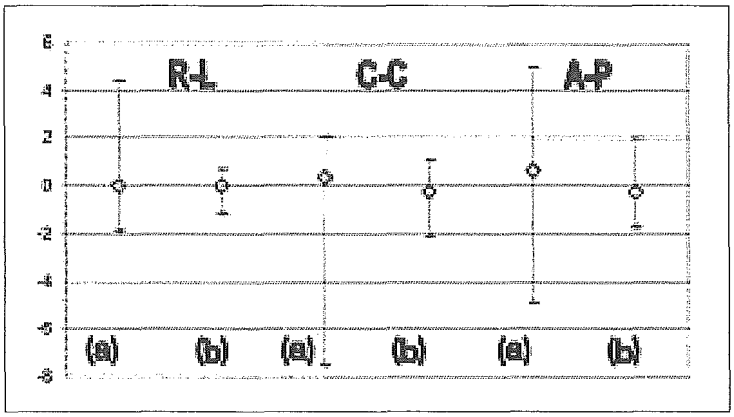

Fig. 4. Comparison of distributions (mean with extremes) of the isocenter displacements by axis from the start of treatment to "off-range" marker position, (◇, a) and the effect of the image-guided reposition protocol (◇, b). The latter corresponds to the actual organ motion under which radiation was delivered, including after last field marker distributions, for intratreatment repositioned sessions. All dimensions are in millimeters.

The intrafraction "repositioning" method was used only one time in >95% of fractions. None of the treatment fractions required repositioning more than twice.

Post-treatment organ motion

Overall distribution plots of the intrafractional error and target location after repositioning was performed during delivery are displayed in Fig. 4, with error bars indicating maximum movement. At treatment completion, O-R coordinates were seen in 29.9% of all fractions (64/214); this included "non-repositioned" fractions, where the majority of shifts were registered: 22.9%, compared with 7% for the repositioned ones. The mean±SD of marker discrepancy for after last field delivery relative to the system isocenter position was 0.02±0.44 mm, −0.14±0.55 mm, and −0.16±0.53 mm in the R-L, C-C, and A-P directions, respectively. All isocenter shifts registered at post-treatment were seen toward both directional components (±). Even though displacements were encountered, they were small in magnitude. Comparable distribution patterns were seen for all patients in this study.

The overall fraction delivery time from setup start to the last field delivered was calculated to be 15±3 minutes, with a tendency to decrease with the amount of treatment experience of the patients and staff.

Discussion

This report presents the measurement and evaluation of inter- and intrafraction organ motion based on a newly developed on-board imaging system capable of KV registration of GS, implanted as fiducial markers, into the prostate. The accuracy of the system was sufficient to assess treatment location errors and allow error corrections. This approach was clinically implemented along with intensity modulated radiation therapy (a tool that provides power to establish and manipulate dissymmetric gradients). The seed implantation procedure was determinant and clinically feasible without any complication or toxicity. Similar methods have been used and reported by Sandler *et al.*,[31] Murphy *et al.*,[32] and Shipley.[33]

For over a decade, efforts to reproduce normal tissues, bone anatomy, and artifact images (fiducial markers) for precise guidance of beam alignment have been made using MV imaging on flat panels and KV sources, the latter having been integrated into the linear accelerator.[34-37] Research results of both approaches clearly show superior performance of KV images in terms of signal-to-noise ratio versus dose, on the flat panel imager, as reported by Groh *et al.*[38] Another advantage is that less energy is required to visualize such structures.

The introduction of this on-board imaging system to clinics was to substantially "abolish" systematic and random error associated with daily positioning and intratreatment. Our system integrates a flat panel detector of 17.9×23.8 cm with dual x-ray sources capable of KV. Previous studies have ascertained the accuracy and stability of this system after software compensation.[28,29] While technical considerations and QA/QC are strictly controlled, the time exposure to X-rays is considered limited and practically similar or less than other methods used[39,40] because of low time exposure. Recently, Jaffray *et al.*[41] integrated a larger-area flat panel detector on a Linac for fluoroscopy, radiography and cone-beam volumetric CT; this technology has been introduced into clinical use, as outlined by Uematsu *et al.*[42]

It must be pointed out that image-guided radiation therapy (IGRT) requires the selection of appropriate target-volume margins and automatized documentation software, among others.

We observed that the patient immobilization method may have a positive impact on patient setup stability and intrafraction motion task; the condition of rectum and bladder filling also plays a protagonistic role that needs to be considered because of its anatomical geometric inconsistency. Nevertheless, this consideration is less imperative when using on-line image-guided technology.

Adequate tumor coverage will depend not only on the immobilization of patients and large "safety" margins used for PTV but also on the reproducibility of intratreatment verification techniques, with the concept of IGRT.

A variety of approaches has been used in regard to the necessity of maintaining the prostate under the desired prescribed dose. In a report of a study involving 772 prostate cancer patients, Teh *et al.*[43] found that in the postoperative pathological findings of the radial distance of extracapsular extension, a 5 mm margin would provide sufficient coverage of the tumor volume, especially in the setting of IMRT treatment.

The patient's daily setup and intrafractional positional verification displacements relative to the system isocenter can be corrected for optimal radiation treatment complemented with a strict allowance for organ shift. Innovative strategies tend to minimize variability in organ motion through techniques implemented in linear accelerators or in treatment rooms. Shimizu *et al.*[15] used a set of four diagnostic x-ray sources and a TV system as the prototype for tracking a GS implanted in 10 prostate tumors and five bladder tumors, intending to remove all intrafractional dislocations. In that study organ motion was found have median absolute values of 0.6 mm, 0.85 mm, and 0.7 mm for the R-L, C-C, and A-P directions, respectively. In our present study, marker coordinate registration, done after every field, showed mean absolute values in the range of 0.45 mm, 1.45 mm, and 1.08 mm in the R-L, C-C, and A-P directions, respectively. Both studies showed larger organ shifts towards the caudal direction. In our opinion, results obtained by the intrafraction repositioning method represent the most realistic parameters of organ motion.

Another technique that has been suggested recently is a US-based daily positional verification of prostate gland position, as reported by different authors.[10,11,13,14] Morr *et al.*[12] reported patient setup average adjustments of 2.6±2.1 mm, 4.2±2.8 mm, and 4.7±2.7 mm in the R-L, C-C, and A-P axis, respectively. A study from Huang *et al.*[10] involving 20 patients, showed an intrafraction mean magnitude of shift (±SD) of 0.01±0.4 mm, 0.1±1.0 mm, and 0.2±1.3 mm in the R-L, C-C, and A-P directions, respectively. A more recent study using US-based daily prostate localization in 17 patients showed an interfraction overall mean target shift of 0.5-0.7 mm in all directions.[11] Compared to our study, their accuracy was limited to a set of conditions including good bladder filling, radiotherapist experience, and the amount of planner pressure against the patient's abdominal wall. As can be seen by comparing the motion data from our study and the US study, organ motion in our investigation was considerably less. Nederveen *et al.*[44] reported a study of 10 prostate cancer patients' intrafraction motion data using an implanted gold marker in the prostate and registered by movie during each fraction. Their findings differed from ours in that the tendency of motion was to the posterior direction; instead, our data pointed to a tendency to shift in the caudal direction. Nevertheless, we cannot ignore the fact that displacements in the posterior axis were registered as well.

Motion error can be corrected satisfactorily, as presented here, with actual translation ranges that are, to our knowledge, among the lowest to have been reported in this area of research.

The major shift concern relies on seed migration; we studied the influence of seed migration and found it to be present within a range of 0-1.2 mm as measured by an algebraic calculation among distances between each of the three GS' coordinates (data not shown). Seed migration has already been reported elsewhere[15] and found to be about 1 mm. Nonetheless, some extra sources of uncertainty could arise owing to differences in the size, shape, or method of insertion of the fiducial markers.

A time-trend organ motion measurement study, during the intrafractional period, showed higher shifts to the caudal and posterior directions, with a tendency to remain constant by the end of the treatment.[18] In our study, a similar pattern was seen for both the repositioned and non-repositioned patients. We also found low variation in mean isocenter shifts following the last radiation field delivery (after Field V). Even though the end of treatment involves certain systematic error considerations like the influence of rectum and bladder filing, the lesser motion seen could indicate an advantage of the initial patient immobilization approach, the hollow-volume condition considerations (rectum/bladder), or the repositioning approach.

The influence of hollow organs on organ motion has been reported through different imaging approaches, some favoring the increase in translations of the prostate[45] or showing low influence in motion.[3] Yeoh *et*

al.[46] found that a low systematic influence of rectum fill on target translations was caused by incontinence induced by the irradiation of rectal tissues. Our assumption that a possible cause might be the patient's sensing the end of treatment has yet to be objectively analyzed.

We have shown that irradiation for moving targets, like the prostate, highlights the need to use imaging tools, like the DFFP system, to avoid inter- intrafraction-induced geometrical target misses. We found that during treatment, 60.7% of prostate organ motion was $<\pm 1$ mm and in 3.5% >3 mm; thus, when using a repositioning method, 99% of all treatment fractions (including those after last field position) was delivered within ± 2 mm of the planned high dose distribution area.

The management of treatment planning margins (CTV/PTV) has been widely overlooked. In the case of PTV size (balance between permissible dose to OAR and targeting accuracy), the probability of coverage based on standard deviation calculation methods[47] and other advanced methods incorporating the geometry of tumors near beam edges[48] or a combination of setup systematic with random error,[49-51] have been formulated as "recipes" for sculpting these global margins. These theoretical calculation methods can help to accomplish treatment for advanced localized peripherally located tumors or groups of patients with extreme prostate size. With a generalized strategy, parts of critical structures may be involved unnecessarily. For this reason, other practical methods like our image-guiding system may become suitable for better target coverage and the reduction of interfraction or intrafraction organ motion.

For a dose-escalation protocol using the IMRT approach, accounting accurately for motion errors through automatic image-processing tools, would avoid the use of wide PTV margins since the markers used are easily registered and target repositions can be made at any time during the treatment course.

In general, prostate treatment encompasses many sources of geographical target misses and, even with new planning technologies (requiring numerous steps) or sophisticated imaging tools, solutions for all motion errors have yet to be found.

Conclusion

Sources of motion uncertainty during high dose radiation therapy for localized prostate cancer were considerably diminished in this study as a result of the use of a promising new technology that has been clinically implemented on a daily basis. Positional corrections of intra-organ GS is feasible, and traditional wider margins for PTV may be unnecessary. This implies potential advancement for safer escalation of doses and better quality of life owing to the possibility of fewer radiation complications. In addition, long-term toxicities, clinical outcomes, and effects from time exposure to radiation need to be clearly established.

Acknowledgements

We would like to give special thanks to all our department colleagues and physics staff for their kind suggestions and collaboration in this investigation protocol.

References

1) Perez AA, Pilepich MV, Zivnuska F. Tumor control in definitive irradiation of localized carcinoma of the prostate. *Int J Radiat Oncol Biol Phys*, 12: 523–531, 1986.
2) Zelefsky MJ, Cowen D, Fuks Z, *et al.* Long term tolerance of high dose three-dimensional conformal radiotherapy in patients with localized prostate carcinoma. *Cancer*, 85: 2460–2468, 1999.
3) van Herk M, Bruce A, Kroes AP, *et al.* Quantification of organ motion during conformal radiotherapy of the prostate by three dimensional image registration. *Int J Radiat Oncol Biol Phys,* 33: 1311–1320, 1995.
4) Crook JM, Raymond Y, Salhani D, *et al.* Prostate motion during standard radiotherapy as assessed by fiducial markers. *Radiother Oncol,* 37: 35–42, 1995.
5) Balter JM, Lam KL, Sandler HM, *et al.* Automated localization of the prostate at the time of treatment using implanted radiopaque markers: technical feasibility. *Int J Radiat Oncol Biol Phys,* 33: 1281–1286, 1995.
6) Alasti H, Petric MP, Catton CN, *et al.* Portal imaging for evaluation of daily on-line setup errors and off-line organ motion during conformal irradiation of carcinoma of the prostate. *Int J Radiat Oncol Biol Phys,* 49: 869–884, 2001.
7) Bergstrom P, Lofrot PO, Widmark A. High-precision conformal radiotherapy (HPCRT) of prostate cancer—a new technique for exact positioning of the prostate at the time of treatment. *Int J Radiat Oncol Biol Phys,* 42: 305–311, 1998.
8) Vigneault E, Pouliot J, Laverdiere J, *et al.* Electronic portal imaging device detection of radioopaque markers for the evaluation of prostate position during megavoltage irradiation: a clinical study. *Int J Radiat Oncol Biol Phys,* 37: 205–212, 1997.
9) Mah D, Freedman G, Milestone B, *et al.* Measurement of intrafractional prostate motion using magnetic resonance imaging. *Int J Radiat Oncol Biol Phys,* 54: 568–575, 2002.
10) Huang E, Dong L, Chandra A, *et al.* Intrafraction prostate motion during IMRT for prostate cancer. *Int J Radiat Oncol biol Phys,* 53: 261–268, 2002.
11) Chandra A, Dong L, Huang E, *et al.* Experience of ultrasound-based daily prostate localization. *Int J Radiat Oncol Biol Phys,* 56: 436–447, 2003.
12) Morr J, DiPetrillo T, Tsai JS, *et al.* Implementation and utility of a daily ultrasound-based localization system with

intensity-modulated radiotherapy for prostate cancer. *Int J Radiat Oncol Biol Phys,* 53: 1124–1129, 2002.
13) Falco T, Shenouda G, Kaufmann C, *et al.* Ultrasound imaging for external-beam prostate treatment setup and dosimetric verification. *Med Dosim,* 27: 271–273, 2002.
14) Trichter F, Ennis RD. Prostate localization using transabdominal ultrasound imaging. *Int J Radiat Oncol Biol Phys,* 56: 1225–1233, 2003.
15) Shimizu S, Shirato H, Kitamura K, *et al.* Use of an implanted marker and real-time tracking of the marker for the positioning of prostate and bladder cancers. *Int J Radiat Oncol Biol Phys,* 48: 1591–1597, 2000.
16) Jaffray DA, Drake DG, Moreau M, *et al.* A radiographic and tomographic imaging system integrated into a medical linear accelerator for localization of bone and soft-tissue targets. *Int J Radiat Oncol Biol Phys,* 45: 773–789, 1999.
17) Ten Haken RK, Forman JD, Heimburger DK, *et al.* Treatment planning issues related to prostate movement in response to differential filling of the rectum and bladder. *Int J Radiat Oncol Biol Phys,* 20: 1317–1324, 1991.
18) Lattanzi J, McNeely S, Hanlon A, *et al.* Daily CT localization for correcting portal errors in the treatment of prostate cancer. *Int J Radiat Oncol Biol Phys,* 41: 1079–1086, 1998.
19) Hanley J, Lumley MA, Mageras GS, *et al.* Measurement of patient positioning errors in three-dimensional conformal radiotherapy of the prostate. *Int J Radiat Oncol Biol Phys,* 37: 435–444, 1997.
20) Lattanzi J, McNeely S, Pinover W, *et al.* A comparison of daily CT localization to daily ultrasound-based system in prostate cancer. *Int J Radiat Oncol Biol Phys,* 43: 719–725, 1999.
21) Zelefsky MJ, Leibel SA, Burman CM, *et al.* Neoadjuvant hormonal therapy improves the therapeutic ratio in patients with bulky prostatic cancer treated with three-dimensional conformal radiation therapy. *Int J Radiat Oncol Biol Phys,* 29: 755–761, 1994.
22) Zelefsky MJ, Harrison A. Neoadjuvant androgen ablation prior to radiotherapy for prostate cancer: reducing the potential morbidity of therapy. *Urol,* 49: 38–45, 1997.
23) Yang FE, Chen GT, Ray P, *et al.* The potential for normal tissue dose reduction with neoadjuvant hormonal therapy in conformal treatment planning for stage C prostate cancer. *Int J Radiat Oncol Biol Phys,* 33: 1009–1017, 1995.
24) Gleason DF. Histologic grading and clinical staging of prostatic carcinoma. In *Urologic pathology. The prostate.* (Tannenbaum M ed.; Lea & Febiger, Philadelphia), pp. 171–197, 1977.
25) International Union Against Cancer (UICC). *TNM Classification of Malignant Tumors,* 5th ed. (Sobin LH, Wittekind Ch eds.; John Wiley & Sons Inc, New York), 1997.
26) Roeske JC, Forman JD, Mesina CF, *et al.* Evaluation of changes in the size and location of the prostate, seminal vesicles, bladder, and rectum during a course of external beam radiation therapy. *Int J Radiat Oncol Biol Phys,* 33: 1321–1329, 1995.
27) ICRU Report No 50: International Commission on Radiation Units and Measurements. *Prescribing, recording, and reporting photon beam therapy.* Washington, DC, 1993.
28) Takai Y, Mitsuya M, Nemoto K, *et al.* Development of a new linear accelerator with dual X-ray fluoroscopy using amorphous silicon flat panel X-ray sensors to detect a gold seed in a tumor at real treatment position. *Int J Radiat Oncol Biol Phys,* 51 (Suppl.): 381, 2001.
29) Takai Y, Mitsuya M, Nemoto K, *et al.* Development of a real-time tumor tracking system with dmlc with dual X-ray fluoroscopy and amorphous silicon flat panel on the gantry of linear accelerator. *Int J Radiat Oncol Biol Phys,* 54: (Suppl.): 193–194, 2002.
30) Wong J. Methods to manage respiratory motion in radiation treatment. American Association of Physicists in Medicine (AAPM). *Medical physics monograph No. 29; Intensity Modulated Radiation Therapy, the state of the art.* (Jatinder R Palta, T Rockwell Mackie eds.; Medical Physics Publishing), Madison WI, pp. 682–685, 2003.
31) Sandler HM, Bree RL, McLaughlin PW, *et al.* Localization of the prostatic apex for radiation therapy using implanted markers. *Int J Radiat Oncol Biol Phys,* 27: 915–919, 1993.
32) Murphy DJ, Porter AT. Prostate localization for the treatment planning of prostate cancer: a comparison of two techniques. *Med Dosim,* 13: 11–12, 1988.
33) Shipley WU. The advantage of an X-ray visible marker of the prostatic apex. *Int J Radiat Oncol Biol Phys,* 27: 985, 1993.
34) Brahme A, Lind B, Nafstadius P. Radiotherapeutic computed tomography with scanned photon beams. *Int J Radiat Oncol Biol Phys,* 13: 95–101, 1987.
35) Midgley S, Millar RM, Dudson J. A feasibility study for megavoltage cone beam CT using commercial EPID. *Phys Med Biol,* 43: 155–169, 1998.
36) Ruchala KJ, Olivera GH, Schloesser EA, *et al.* Megavoltage CT on a tomography system. *Phys Med Biol,* 44: 2597–2621, 1999.
37) Jaffray DA, Drake DG, Moreau M, *et al.* A radiographic and tomographic imaging system integrated into a medical linear accelerator for localization of bone and soft-tissue targets. *Int J Radiat Oncol Biol Phys,* 45: 773–789, 1999.
38) Groh BA, Siewerdsen JH, Drake DG, *et al.* A performance comparison of flat-panel imager-based MV and KV cone-beam CT. *Med Phys,* 29: 967–975, 2002.
39) Shirato H, Shimizu S, Kunieda T, *et al.* Physical aspects of a real-time tumor-tracking system for gated radiotherapy. *Int J Radiat Oncol Biol Phys,* 48: 1187–1195, 2000.
40) Low DA, Zhu XR, Purdy JA, *et al.* The influence of angular misalignment on fixed-portal intensity modulated radiation therapy. *Med Phys,* 24: 1123–1139, 1997.
41) Jaffray DA, Siewerdsen JH, Wong JW, *et al.* Flat-panel cone-beam computed tomography for image-guided radiation therapy. *Int J Radiat Oncol Biol Phys,* 53: 1337–1349, 2002.
42) Uematsu M, Shioda A, Tahara K, *et al.* Focal, high dose,

and fractionated modified stereotactic radiation therapy for lung carcinoma patients: a preliminary experience. *Cancer,* 82: 1062–1070, 1998.
43) Teh BS, Bastasch MD, Wheeler TM, *et al.* IMRT for prostate cancer: defining target volume based on correlated pathologic volume of disease. *Int J Radiat Oncol Biol Phys,* 56: 184–191, 2003.
44) Nederveen AJ, van der Heide UA, Dehnad H, *et al.* Measurements and clinical consequences of prostate motion during a radiotherapy fraction. *Int J Radiat Oncol Biol Phys,* 53: 206–214, 2002.
45) Melian E, Kutcher GJ, Zelefsky MJ, *et al.* Variation in prostate position quantitation and implications for three-dimensional conformal treatment planning. *Int J Radiat Oncol Biol Phys,* 38: 73–81, 1997.
46) Yeoh EE, Botten R, Russo A, *et al.* Chronic effects of therapeutic irradiation for localized prostatic carcinoma on anorectal function. *Int J Radiat Oncol Biol Phys,* 47: 915–924, 2000.
47) Goitein M, Schultheiss TE. Strategies for treating possible tumor extension: some theoretical considerations. *Int J Radiat Oncol Biol Phys,* 11: 1519–1528, 1985.
48) Fontenla E, Pelizzari CA, Chen GT. Implications of 3-dimmensional target shape and motion in aperture design. *Med Phys,* 23: 1431–1441, 1996.
49) Antolak JA, Rosen II. Planning target volumes for radiotherapy: how much margin is needed? *Int J Radiat Oncol Biol Phys,* 44: 1165–1170, 1999.
50) Stroom JC, de Boer HC, Huizenga H, *et al.* Inclusion of geometrical uncertainties in radiotherapy treatment planning by means of coverage probability. *Int J Radiat Oncol Biol Phys,* 43: 905–919, 1999.
51) van Herk M, Remeijer P, Rasch C, Lebesque JV. The probability of correct target dosage: dose-population histograms for deriving treatment margins in radiotherapy. *Int J Radiat Oncol Biol Phys,* 47: 1121–1135, 2000.

Atsuya Takeda, MD
Etsuo Kunieda, MD, PhD
Naoyuki Shigematsu, MD, PhD
Deloar M. Hossain, PhD
Takatsugu Kawase, MD
Toshio Ohashi, MD
Jun-ichi Fukada, MD
Osamu Kawaguchi, MD
Minoru Uematsu, MD, PhD[2]
Toshiaki Takeda, MD
Kazuhiko Takemasa, MD, PhD
Takeshige Takahashi
Atsushi Kubo, MD, PhD

Published online before print
10.1148/radiol.2371032102
Radiology 2005; 237:295–300

[1] From the Dept of Radiology (A.T., E.K., J.F., T. Takeda, K.T., T. Takahashi), Tokyo Metropolitan Hiro-o General Hosp, Tokyo, Japan; Dept of Radiology, Keio Univ, 35 Shinanomachi, Shinjyuku, Tokyo 160-8582, Japan (E.K., N.S., D.M.H., T.K., T.O., J.F., O.K., A.K.); Japan Science and Technology Agency, CREST, Tokyo, Japan (E.K., D.M.H., T.K., O.K.); and Dept of Radiation Oncology, National Defense Medical College, Saitama, Japan (M.U.). Received Dec 27, 2003; revision requested Feb 27, 2004; final revision received Sept 10; accepted Nov 11. Address correspondence to E.K.

Authors stated no financial relationship to disclose.

Current address:
[2] Dept of Radiology, Keio Univ

Author contributions:
Guarantors of integrity of entire study, A.T., E.K.; study concepts and design, A.T., E.K.; literature research, A.T., E.K.; clinical studies, A.T., E.K., T. Takeda, J.F., T. Takahashi, K.T.; data acquisition, N.S., M.U., T.O., J.F., O.K., T.K.; data analysis/interpretation, A.T., E.K., D.M.H., T. Takeda, K.T., T. Takahashi, A.K.; statistical analysis, A.T., E.K., D.M.H.; manuscript preparation, M.U., N.S., T.O.; manuscript definition of intellectual content, A.T., E.K., J.F., O.K., T.K., D.M.H.; manuscript editing, A.T., E.K., T. Takeda, K.T., T. Takahashi, A.K.; manuscript revision/review, A.T., E.K., N.S., T.O., J.F., D.M.H., O.K., T. Takeda; manuscript final version approval, all authors

Small Lung Tumors: Long-Scan-Time CT for Planning of Hypofractionated Stereotactic Radiation Therapy—Initial Findings[1]

PURPOSE: To prospectively use long-scan-time computed tomography (CT) to visualize the trajectory of tumor movements or the internal target volume.

MATERIALS AND METHODS: The study was approved by the institutional review board. Written informed consent was obtained from participants after the study and the role of procedures were explained fully. During the planning of stereotactic radiation therapy for 10 patients (nine men, one woman; mean age, 77 years; range, 69–89 years) with small lung tumors (mean volume, 9.0 cm^3; range, 3.6–24.9 cm^3), fluoroscopic imaging, long-scan-time CT, and thin-section CT were performed. The tumor and the partial-volume-averaging effects that resulted from tumor movement were delineated on each section at long-scan-time CT performed during the patient's steady breathing with scan time of 8 seconds per image. Visualized internal target volume was defined by integrating the sections. A simple model was examined for estimating internal target volume on the basis of respiratory motion and gross target volume delineated on thin-section CT images. Visualized internal target volume and estimated internal target volume were compared quantitatively and graphically. The Mann-Whitney test was used to analyze the relation between gross target volume delineated on thin-section CT images and the ratio of visualized internal target volume to the defined gross target volume.

RESULTS: The correlation coefficient between visualized internal target volume and estimated internal target volume was $r = 0.98$ ($P < .001$). The mean relative error ± standard deviation was 1.9% ± 19.0 (range, −11.0% to 56.4%). Excluding one case with an irregularly shaped tumor (56.4%), the mean relative error was −4.1% ± 4.1. In patients with small tumors (defined gross target volume, ≤10 cm^3), the ratio of the visualized internal target volume to the defined gross tumor volume was significantly larger than that in patients with larger tumors (1.2–2.0 vs 1.0–1.2; $P < .05$). In some cases in which marginal spiculation depicted on thin-section CT images was blurred on long-scan-time CT images, the blurred area was erroneously excluded from the target volume.

CONCLUSION: In most cases, values for visualized internal target volume and estimated internal target volume were similar and long-scan-time CT depicted virtually the entire tumor trajectory.

Stereotactic radiosurgery performed by delivering a high dose of concentrated gamma rays or x-rays is one of the major strategies for treating intracranial lesions, and favorable results with fractionated stereotactic radiation therapy have been reported for some malignant and benign tumors (1,2). Hypofractionated stereotactic radiation therapy (ie, radiation therapy administered in a small number of dose fractions) has been applied to treat extracranial lesions as well (3–7). In a preliminary report (7), excellent results were

reported, including a local control rate of 94% and a 3-year cause-specific survival of 88%, after body stereotactic radiation therapy with a dose of 50 Gy administered in five fractions in patients with early-stage primary lung cancer.

For successful treatment with stereotactic radiation therapy, it is crucial to obtain accurate information about the tumor position and potential range of movement, since a concentration of beams from several different directions delivers a very high dose to the target volume, whereas there is a steep decrease in dose at the margins of the targeted area (8). Stereotactic radiation therapy for lung lesions, unlike stereotactic irradiation for intracranial lesions, entails inevitable problems, such as movement of the target because of respiratory and cardiac motion. In particular, respiration-related movement, which is often greater than 1 cm, is clinically important for lung stereotactic radiation therapy, since the diameter of lung lesions treated with this method is typically less than 4 cm.

The conventional method for planning radiation therapy of small lung tumors usually involves the use of CT and, if required, fluoroscopy to visualize the respiration-related movement of the lesion. More specifically, we conventionally obtain the gross tumor volume measurements with CT while the patient performs breath holding after inhalation, a method that does not allow tumor movement to be taken into account. Tumor movement in the craniocaudal direction during breathing is observed with fluoroscopy in the anteroposterior view, and, finally, the degree of tumor movement is added as an internal margin to the gross tumor volume to obtain the internal target volume.

The addition of the internal margin to the gross tumor volume is difficult, however, because the internal margin is not visible on CT images obtained with breath holding. If too narrow an internal margin is applied so as to reduce the adverse effects of radiation therapy, the dose distribution might be too restricted to compensate for tumor movement. Equally, if too wide a margin is used, the increased size of the target volume might result in an increased risk for radiation-induced injury to normal tissue. Moreover, it is virtually impossible to evaluate three-dimensional movement of the tumor with fluoroscopy.

To visualize the internal target volume for planning of stereotactic radiation therapy in lung tumors, we therefore used long-scan-time CT. Our hypothesis was that it would be possible to use long-scan-time CT to demonstrate a major part of the trajectory of tumor movement due to respiration and other factors. This hypothesis was based on the longer duration of scanning with this method, in comparison with scan time at conventional CT. If our hypothesis was correct, the internal target volume would be depicted by using long-scan-time CT, and we expected this method to facilitate the straightforward delineation of the planning target volume by adding an adequate margin to the visualized internal target volume (Fig 1).

Thus, the purpose of our study was to prospectively use long-scan-time CT to define the trajectory of tumor movement, or the internal target volume.

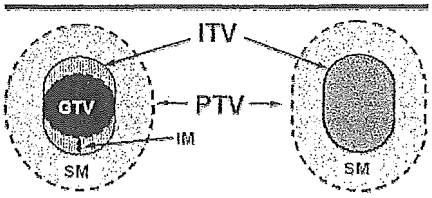

Figure 1. Left: Diagram of standard treatment planning method based on gross tumor volume *(GTV)* defined with breath-hold thin-section CT. With this method, the range of tumor motion is depicted only in the craniocaudal direction, and the internal margin *(IM)* is used to define the internal target volume *(ITV)*. Right: Diagram of alternative planning method in which the internal target volume, including the internal margin, is determined directly with long-scan-time CT. The setup margin *(SM)* is added to the internal target volume in order to define the planning target volume *(PTV)*.

MATERIALS AND METHODS

Patients

Ten patients with small lung tumors (<4 cm in diameter) were recruited for the study between December 2001 and July 2002. Nine men and one woman with a mean age of 77 years (range, 69–89 years) were included. The tumors consisted of eight primary lung cancers and two solitary pulmonary metastases. Patients with primary lung cancer had no evidence of metastasis to regional lymph nodes or of distant metastasis. Those with pulmonary metastasis had no evidence of other metastases, and the primary lesions were controlled. The mean tumor volume was 9.0 cm^3 (range, 3.6–24.9 cm^3). A diagram of tumor locations in the lung of individual patients is shown in Figure 2. The study was approved by the institutional review board. Written informed consent was obtained from each participant after the study and role of the procedures had been fully explained.

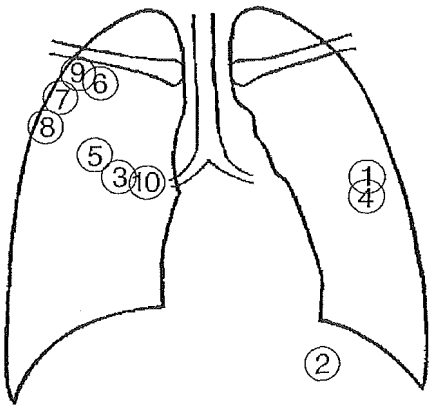

Figure 2. Diagram shows location of lung tumor in each patient. Circled numbers represent the patient numbers (Table).

Fluoroscopic Measurement and CT Imaging

An integrated radiation therapy simulator equipped with a fluoroscopic unit (KXO-50 N; Toshiba, Tokyo, Japan), and a single-detector row CT scanner (X Vigour; Toshiba), were used in this study. Patients were instructed to breathe shallowly and evenly when undergoing fluoroscopic imaging and long-scan-time CT. If breathing-related tumor movement on anteroposterior fluoroscopic scout images was greater than 1 cm, a corset was used to restrict the patient's abdomen and reduce diaphragmatic movement. Then fluoroscopy was performed with a source-to-tumor distance of 100 cm, and breathing-associated tumor movement in the craniocaudal direction was measured by a radiation oncologist (A.T.) using a ruler installed on the fluoroscopic unit. All the tumors were depicted at fluoroscopy.

Long-scan-time CT was performed to enable visualization of the tumor within its entire trajectory during breathing-related movement (scan length, approximately 20 mm). A section thickness of 2 mm (120 kVp, 400 mAs) and scan time of 8 seconds per section were used; this period exceeded the duration of one respiratory cycle in all patients. Conventional thin-section CT was performed with patient breath holding, section thickness of 2 mm (pitch of 1, 120 kVp, 200 mAs), and scan time of 1 second per section.

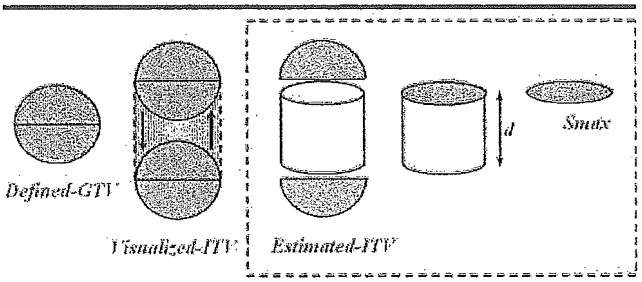

Figure 3. Diagram of defined gross tumor volume *(GTV)*, visualized internal target volume *(ITV)*, and estimated internal target volume. The maximum area of the tumor delineated on cross-sectional thin-section CT images *(Smax)* and the fluoroscopically measured breathing-induced tumor displacement in the craniocaudal direction *(d)* were used to calculate the tumor trajectory (ie, estimated internal target volume).

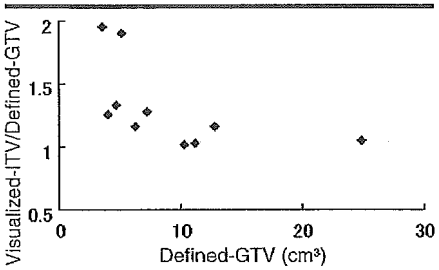

Figure 4. Graph of relation between the visualized internal target volume *(ITV)*/defined gross tumor volume *(GTV)* ratio and the defined gross tumor volume shows that smaller tumors have a larger ratio. This result implies that the treatment planning target volume must be determined more carefully prior to treatment of small tumors with stereotactic radiation therapy.

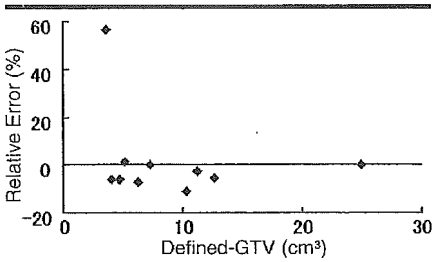

Figure 5. Scatterplot shows relation between defined gross tumor volume *(GTV)* and relative error in the study sample. For one tumor, there was a relative error of approximately 60%. For all the others, the relative error approached 0% (horizontal line) or was negative.

Target Volume Definition and Analysis

Images obtained with the two procedures just described were displayed on a planning workstation monitor with the window width set at 1500 HU and the window level at −600 HU. On thin-section CT images, a radiation oncologist (A.T.) with 10 years of experience in radiation oncology delineated the tumor contours (Sc) in each section and defined the maximum tumor area as S_{max}. On long-scan-time CT images, the tumor trajectory (Sl) was outlined on each section that included the tumor, which appeared as a solid mass with partial-volume-averaging effect due to motion. If the image showed an area with attenuation slightly higher than that of adjacent lung tissue, we included that area in the target volume. We did not consider the thin-section CT images while outlining the tumor trajectory on the long-scan-time CT images. The defined gross tumor volume and visualized internal target volume were calculated on the basis of thin-section CT images and long-scan-time CT images, respectively, by using the following equations:

$$GTV_{def} = \sum Sc \cdot h, \quad (A)$$

and

$$ITV_{vis} = \sum Sl \cdot h, \quad (B)$$

where GTV_{def} is the defined gross tumor volume, ITV_{vis} is the visualized internal target volume, and h denotes the section thickness (2 mm) for thin-section CT and long-scan-time CT. Then the estimated internal target volume (ITV_{est}) was calculated on the basis of S_{max}, GTV_{def}, and d (the fluoroscopically measured craniocaudal distance of breathing-related tumor movement), with $ITV_{est} = GTV_{def} + (S_{max} \cdot d)$ (Fig 3).

To examine the relation between the visualized internal target volume and the estimated internal target volume, we compared the two by calculating the relative error (RE) as a percentage, with $RE = (ITV_{vis} - ITV_{est})/ITV_{est} \cdot 100$ (4).

We analyzed the relation between the defined gross tumor volume and the ratio of the visualized internal target volume to the defined gross tumor volume, as well as the relation between the defined gross tumor volume and the relative error.

In all patients, the imaging features of the lesions on long-scan-time CT images and thin-section CT images were analyzed by the same radiation oncologist (A.T.).

Statistical Analysis

The Mann-Whitney test was used to analyze the relation between the defined gross tumor volume and the ratio of the visualized internal target volume to the defined gross tumor volume. Spreadsheet software (Excel 2002; Microsoft, Bellingham, Wash) and a commercial software program for statistical analysis (Statcel, version 1.1, 2002; OMS Publishing, Tokyo, Japan) were used.

RESULTS

The measured and estimated values of the internal target volume in patients are shown in the Table. The mean ± standard deviation for the distance of respiratory-related tumor movement was 4.4 mm ± 3.9 (range, 1–15 mm); for maximum tumor area, 5.2 cm^2 ± 2.7 (range, 2.9–11.7 cm^2); for defined gross tumor volume, 9.0 cm^3 ± 6.4 (range, 3.6–24.9 cm^3); for estimated internal target volume, 10.9 cm^3 ± 6.4 (range, 4.5–26.1 cm^3); and for visualized internal target volume, 10.8 cm^3 ± 6.1 (range, 5.1–26.1 cm^3). The coefficient for correlation between the estimated internal target volume and visualized internal target volume was $r = 0.98$ ($P < .001$).

The relation between the defined gross tumor volume and the ratio of the visualized internal target volume to the defined gross tumor volume is shown in Figure 4. For patients with small tumors with a defined gross tumor volume of 10 cm^3 or less, the ratio of the visualized internal target volume to the defined gross tumor volume was significantly greater (1.2–2.0) than that for patients with larger tumors (1.0–1.2) ($P < .05$).

The relation between defined gross tumor volume and relative error is shown in Figure 5. The relative error ranged from −11.0% to 56.4%, and the mean was 1.9% ± 19. Typical examples of tumor delineation on thin-section and long-scan-time CT images are shown in Figure 6, *A* and *B*, respectively.

Comparison between Estimated and Visualized Internal Target Volumes

Patient No.	Tumor Motion* (mm)	Maximum Tumor Area† (cm^2)	Defined Gross Tumor Volume (cm^3)	Estimated Internal Target Volume	Visualized Internal Target Volume	Relative Error (%)	ITV_{vis}/GTV_{def} Ratio‡
1	4	4.07	6.25	7.88	7.31	−7.23	1.25
2	15	3.02	5.15	9.68	9.82	1.44	1.33
3	4	5.06	7.26	9.29	9.30	0.10	1.94
4	4	7.49	12.73	15.73	14.79	−5.73	1.16
5	3	2.94	3.59	4.48	7.14	56.47	1.28
6	4	3.38	4.03	5.38	5.07	−5.76	1.90
7	3	4.88	10.34	11.80	10.53	−11.01	1.01
8	5	3.97	4.69	6.68	6.26	−6.28	1.02
9	1	5.82	11.24	11.82	11.51	−2.54	1.16
10	1	11.71	24.89	26.06	26.05	0.00	1.04
Mean for all patients	4.4	5.23	9.02	10.88	10.76	1.95	1.31

* Breathing-induced tumor displacement in the craniocaudal direction was measured with fluoroscopy.
† Tumor area was measured on thin-section CT images.
‡ Ratio of the visualized internal target volume to the defined gross tumor volume.

The relative error for patient 5 was 56.4%. On thin-section CT images in this patient, the shape of the tumor was irregular and complex (Fig 7, *A–D*). Figure 7, *E*, shows the tumor delineation on a long-scan-time CT image. In this case, the appearance of the tumor in corresponding and adjacent tumor sections on thin-section CT images (Fig 7, *F–H*) differed markedly from that on long-scan-time CT images. If patient 5 is excluded, the mean relative error is −4.1% ± 4.1.

For patient 7, a large negative relative error of −11.0% was found. The thin-section CT images showed fine spiculation, consolidation, and emphysematous changes surrounding the nodule. On the long-scan-time CT images, however, the tumor margin was depicted with attenuation lower than that on thin-section CT images, was blurred, and was indistinguishable from the surrounding emphysematous changes; consequently, this marginal area was erroneously excluded from the target volume (Fig 8).

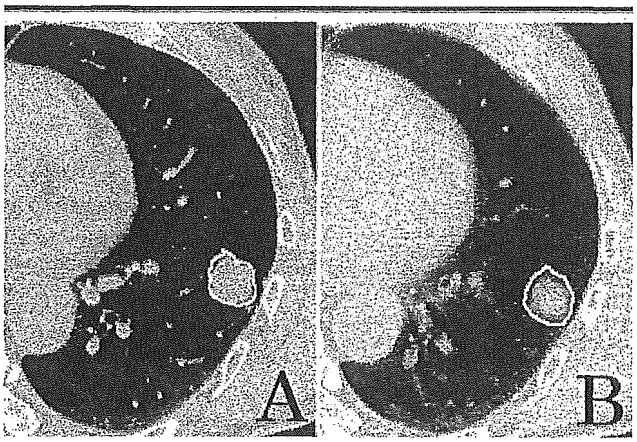

Figure 6. *A*, Transverse breath-hold thin-section CT image shows tumor contour (outline), tumor margin, and bronchovascular bundle. *B*, Transverse long-scan-time CT image shows delineation of tumor movement trajectory (outline) that includes ill-defined tumor margin.

DISCUSSION

With the aim of more precise administration of irradiation, the authors of a report published by the International Commission on Radiation Units and Measurements (9) proposed a new definition of the margin around the target volume to include an internal margin and a so-called setup margin. This explicit definition of tumor margins is particularly important for stereotactic radiation therapy, three-dimensional conformal radiation therapy, and intensity-modulated radiation therapy.

There is no proved rational basis, however, for adding this internal margin to the gross tumor volume, when treatment planning is based on measurements of gross tumor volume with breath-hold thin-section CT. While using this conventional planning method, we observed tumor motion only in the craniocaudal direction with fluoroscopy, and we added the area of this tumor movement to the gross tumor volume, as the internal margin; tumor movement in the anteroposterior and left-to-right directions, however, was not taken into account. The planning target volume that was defined on the basis of the resultant fixed expansion of the gross tumor volume usually was larger than the actual trajectory of tumor motion. When this fluoroscopy-based definition of the planning target volume is used, the defined volume might be too large if tumor movement in the craniocaudal direction is substantial.

Balter and colleagues (10) reported that tumor motion associated with breathing is not negligible and that free-breathing CT studies may erroneously indicate the position and volume of the critical structure and, thus, may lead to faulty planning on the basis of volume-dependent criteria. Since free-breathing CT scans are typically acquired at the rate of one or two sections per second, the individual images might reflect only a limited part of the tumor motion in the respiratory cycle. In comparison, long-scan-time CT was performed at the rate of 8 seconds per section acquired. The duration of scanning was programmed to be sufficiently long (ie, longer than that of the respiratory cycle), and the trajectory of